Thyroid and Endocrine Tumors

11

M. Eiber, F. Gärtner, K. Scheidhauer,
and M. Souvatzoglou

Contents

Thyroid and Endocrine Tumors

In thyroid cancer ^{18}F-FDG is well established for detection of noniodine-avid disease in patients with elevated Tg levels [1, 2]. This has led to a substantial improvement of patient management especially for cases of recurrent tumor [3]. From a prognostic perspective it is known that patients with FDG-avid, high-volume disease (>125 mL) as assessed with CT and PET have markedly reduced survival [4]. Thus FDG PET is a tool for assisting in the clinical decision making for either localized or systemic therapy other than the use of ^{131}I in patients with negative iodine scans and elevated hTg and in patients with suspected local recurrence after thyroidectomy [5]. One important prerequisite of using ^{18}F-PET/CT for these patients is that no intravenous contrast media should be administered when combined with a ^{131}I-scan or when potentially a radio-iodine-therapy is planned no intravenous contrast should be administered for the diagnostic CT [6, 7]. Here PET/MR can offer the possibility to add a diagnostic morphological dataset to the PET/examination as Gd-based contrast media do not interfere with the use of a ^{131}I-scan or therapy. Additionally PET/MR is expected to be a useful tool in surgical planning and radioactive iodine therapy decisions.

For neuroendocrine tumors of the abdomen the use of PET/MR offers potential advances especially for detection of the primary tumor and potential liver metastases. Recently studies [8, 9] showed that ^{68}Ga- radiolabeled somatostatin analog and combination of PET and MR performed significantly more accurate (sensitivity, specificity, NPV, and PPV of 91, 96, 87, and 97 %) compared to PET/CT (74, 88, 69, and 93 %, respectively). It is assumed that MRI compensates for the drawbacks in PET in small hepatic lesions where diffusion-weighted imaging can provide high lesion-to-liver contrast. Additional gain in diagnostic performance is also expected for determining the extent primary pancreatic tumors and thus helping in therapeutic decisions [10, 11]. Especially for neuroendocrine pancreatic cancer MR is often superior to CT in the detection of small lesions implying an important role of PET/MR in this patient population [12, 13].

M. Eiber (✉)
Department of Radiology, Klinikum Rechts der Isar,
Technische Universität München, Munich, Germany
e-mail: matthias.eiber@tum.de

F. Gärtner • K. Scheidhauer • M. Souvatzoglou
Department of Nuclear Medicine,
Technische Universität München, Munich, Germany

O. Ratib et al. (eds.), *Atlas of PET/MR Imaging in Oncology*,
DOI 10.1007/978-3-642-31292-2_11, © Springer-Verlag Berlin Heidelberg 2013

Metastatic Pulmonary Carcinoid

Clinical History

Twenty-nine-year-old male patient with a neuroendocrine tumor of the right upper lobe of the lung, bilobectomy was performed 6 years ago. Resection of a bone metastasis in the proximal right tibia was performed 3 years ago.

Imaging Technique

Whole body PET/MR images acquired 42 min after i.v. injection of 131 MBq [68Ga]-DOTATOC, weight 82 kg. 8 bed positions × 4 min (head to lower legs). MR-Sequences: Whole body: Dixon for attenuation correction, cor T1 TSE. Liver: ax/cor T2 BLADE.

Findings

PET shows disseminated bone metastases with avid tracer uptake, correlating with suspicious hypointense signal alterations on the T1-weighted MR images. Additionally, multiple somatostatin-receptor positive liver metastases are seen, showing hyperintense correlates in the T2-weighted MR images.

Teaching Points

Somatostatin receptor PET/MR is feasible for whole-body staging of patients with neuroendocrine tumors. This patient underwent peptide receptor radiotherapy (PRRT) with Lu-177-DOTATATE.

Fig. 11.1 *Left*: MIP of the [68Ga]-DOTATOC tracer distribution, showing multiple pathologic foci in the bones and in the liver. *Right*: whole-body T1-weighted coronal slice for anatomic overview. Notice attenuation correction artifact of the upper abdomen due to respiratory motion

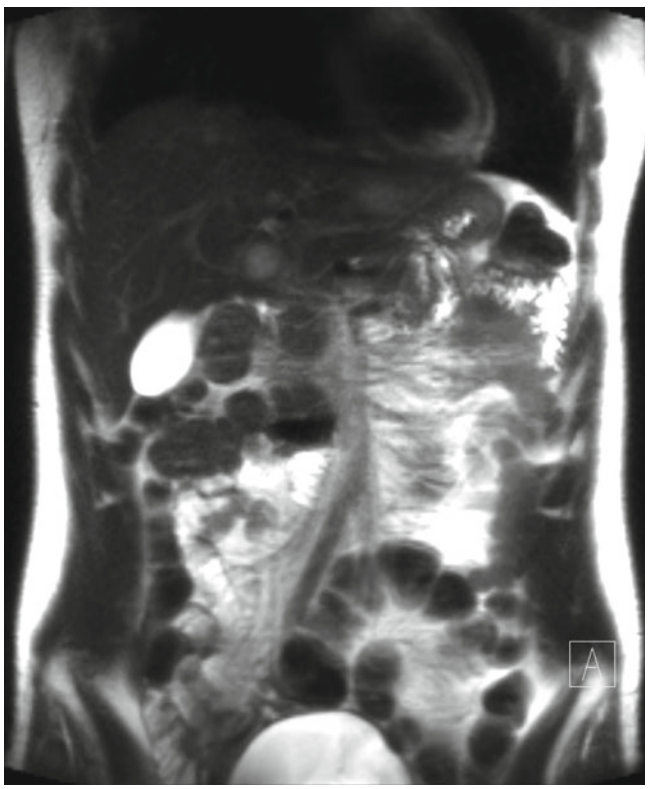

Fig. 11.2 Coronal T2-weighted MRI (BLADE) of the abdomen. Multiple pathologic signal enhancements are seen in the liver, consistent with multiple hepatic metastases

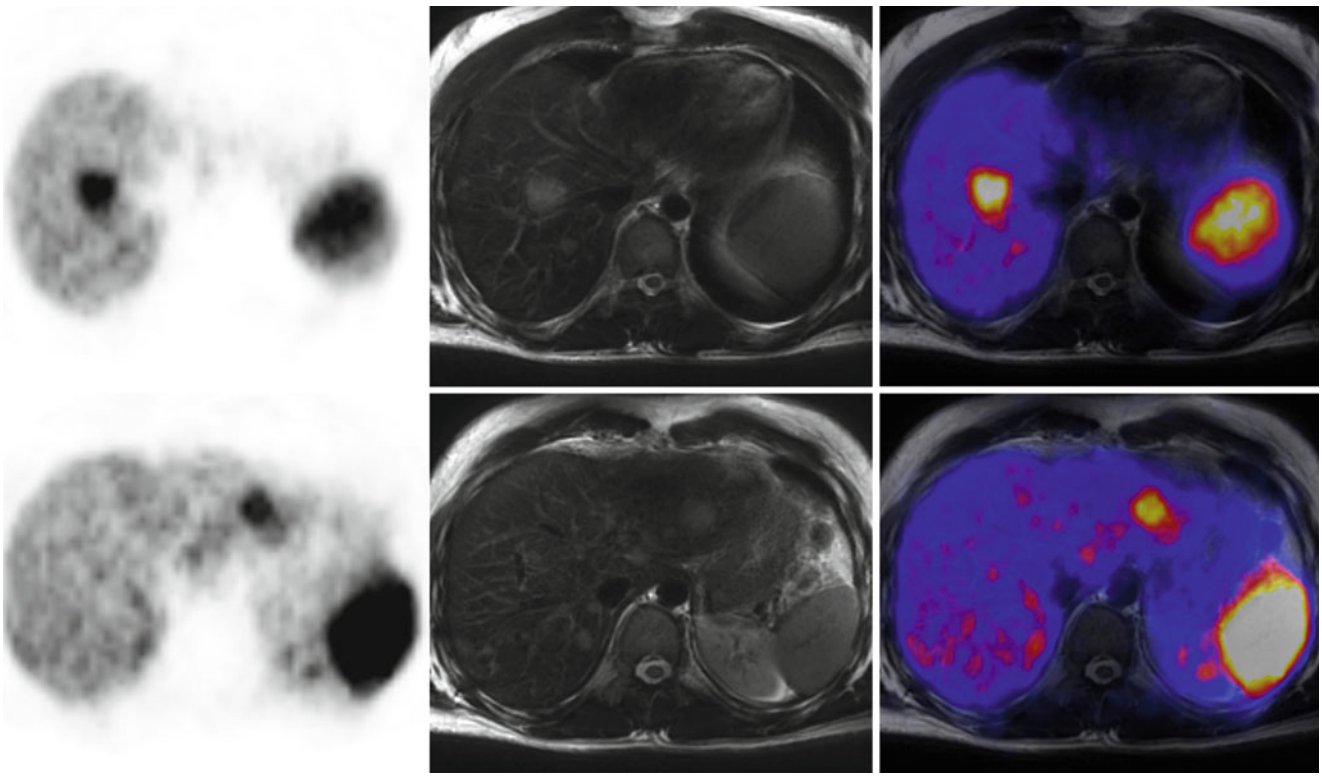

Fig. 11.3 *Left column*: Two axial slices (*top row* and *bottom row*) showing somatostatin-receptor positive liver metastases with intense tracer uptake (PET). *Middle column*: T2-weighted MR images show multiple hyperintense masses in the liver, corresponding to the areas of increased somatostatin receptor expression, consistent with liver metastases. Furthermore, additional multiple smaller hyperintense lesions are seen on the MR images, also suspicious for malignancy. *Right column*: PET/MR fusion

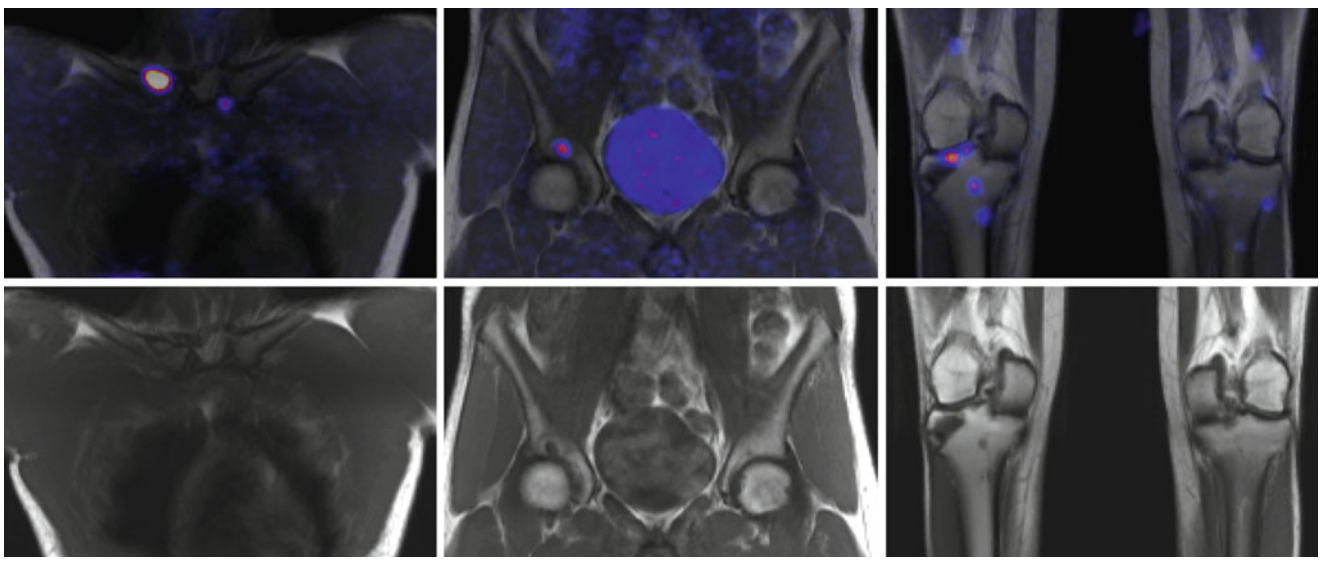

Fig. 11.4 Examples of the multiple bone metastases in this patient. *Top row*: coronal PET/MR fusion. *Bottom row*: coronal T1-weighted MR images. *Left column*: Metastasis in the right clavicle showing intense somatostatin receptor overexpression. *Middle column*: Metastasis in the right acetabulum, showing a a clear hypointense correlate in the T1w MR image. *Right column*: multiple somatostatin-receptor positive bone metastases in the right proximal tibia. Additionally, a large hypointense defect is observed in the T1w MR images in the lateral part of the proximal right tibia, showing no tracer uptake, consistent with postoperative changes

Metastatic Medullary Thyroid Cancer

Clinical History

Eighty-six-year-old male patient with history of total thyroidectomy (medullary thyroid cancer) 12 years ago and radiotherapy of a bone metastasis (4th lumbar vertebra) 2 years ago. Currently ongoing therapy with somatostatin analogs.

Imaging Technique

Whole body PET/MR images acquired 103 min after i.v. injection of 107 MBq [68Ga]-DOTATOC, weight 67 kg. 3 bed positions × 4 min (head to pelvis). MR-Sequences: Partial body: Dixon for attenuation correction, cor T1 TSE. Liver: ax/cor T2 BLADE, ax T1 VIBE, ax DWI.

Findings

Local recurrence and bone metastases showing intense overexpression of the somatostatin-receptor. Disseminated liver metastases are also observed, showing only low to moderate receptor expression.

Teaching Points

DOTATOC PET/MR can be used for assessment of somatostatin-receptor expression of neuroendocrine tumors. Especially in the liver, DWI can help to identify small or receptor-negative lesions.

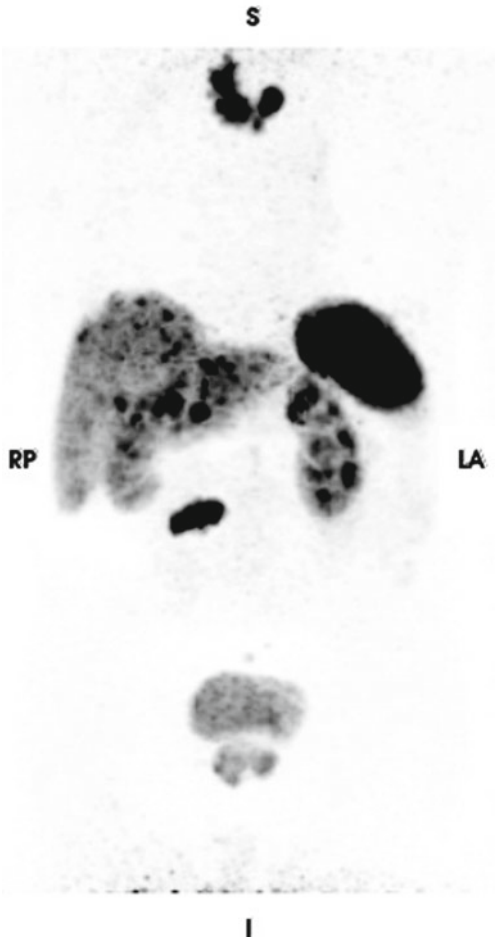

Fig. 11.5 The MIP overview shows pathologic tracer accumulation in the neck, bone (lumbar spine, pelvis) and inhomogeneous uptake in the liver

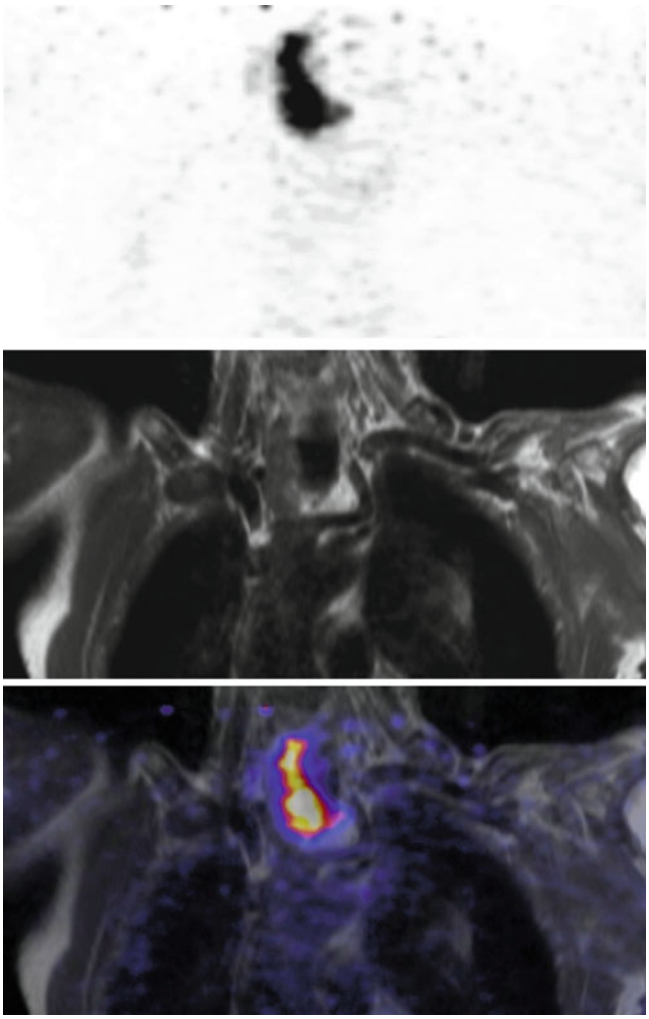

Fig. 11.6 Local recurrence in the area of the right thyroid bed with intense somatostatin receptor expression (PET, *top*). A hypointense mass is seen on coronal T1-weighted MR-images (*middle*). *Bottom*: PET/MR fusion

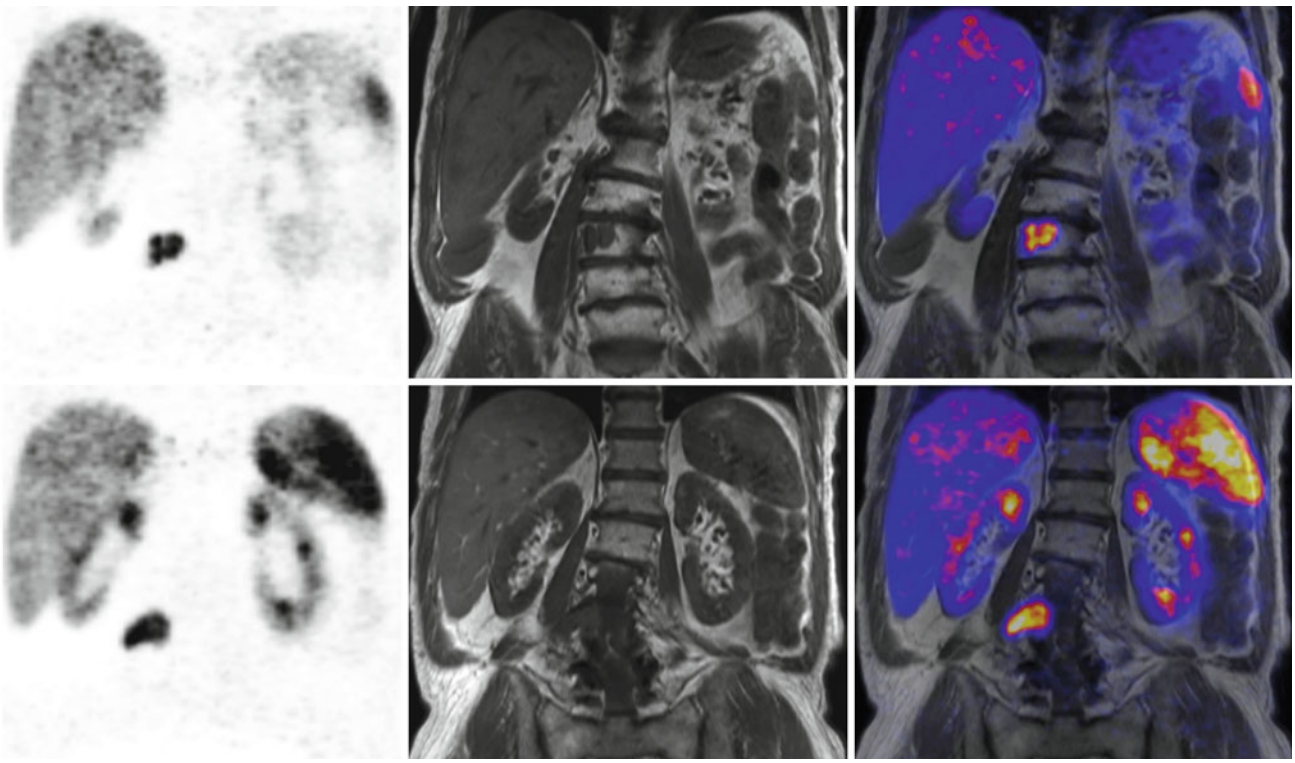

Fig. 11.7 Two coronal views (*top* and *bottom row*) showing a bone metastasis in the 4th lumbar vertebra (lumbalization of the 1st sacral vertebra). *Left*: PET shows intense overexpression of the somatostatin receptor. *Middle*: Hypointense mass in the 4th lumbar vertebra with extrasseous soft tissue extension to the right side. *Right*: PET/MR fusion

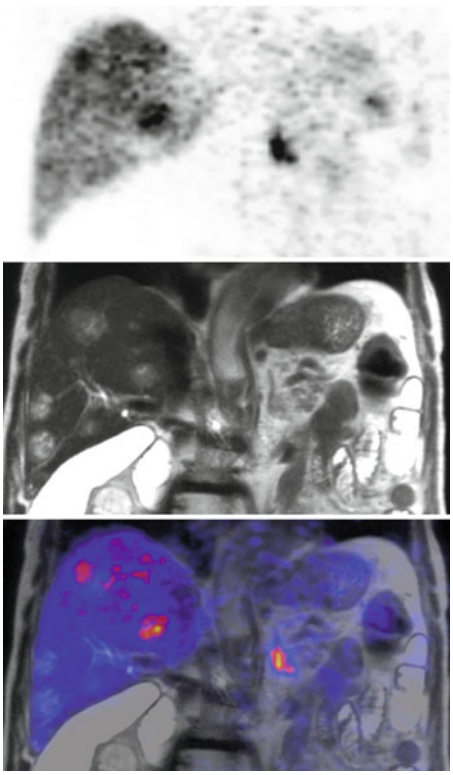

Fig. 11.8 Multiple liver metastases, partly somatostatin receptor positive. *Top*: coronal PET. *Middle*: coronal T2 BLADE MRI. *Bottom*: PET/MR fusion

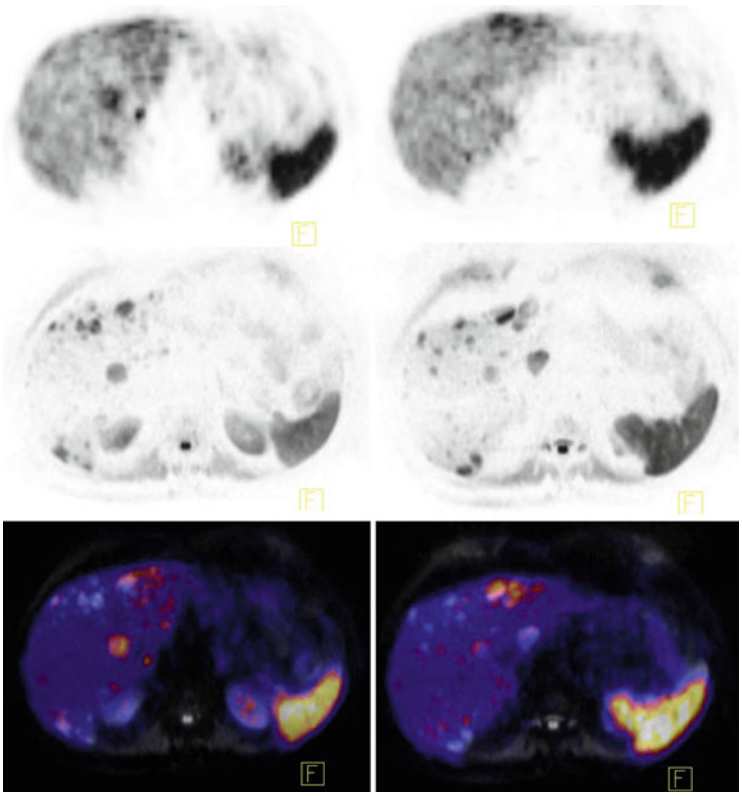

Fig. 11.9 Two axial slices (*left* and *right column*) showing multiple liver metastases. *Top*: some metastases show low to moderate expression of the somatostatin receptor (PET). *Middle*: diffusion-weighted MRI (DWI, $b=800$) additionally shows disseminated small, receptor negative metastases. *Bottom*: PET/MR fusion

Benign Finding on Somatostatin Receptor PET/MR

Clinical History

Fifty-one-year-old male patient after resection of a medullary thyroid carcinoma (left thyroid lobe, T2 N0 M0 R0) including neck dissection two years ago. The serum calcitonin was 72 ng/ml at the time of PET/MR imaging.

Imaging Technique

Partial body PET/MR images acquired 84 min after i.v. injection of 129 MBq [68Ga]-DOTATOC, weight 70 kg. 3 bed positions × 4 min (head to pelvis). MR-Sequences: Dixon for attenuation correction, cor T1w, sag T1w (spine) and sag T2w (spine) sequences.

Findings

Moderate tracer accumulation in the 8th thoracal vertebra. No further foci of pathological tracer accumulation. The finding correlates with a hyperintensity in the T1w images and in the fat-weighted Dixon images, corresponding to an hemangioma. The study was rated negative for metastases.

Teaching Points

MRI is useful to further characterize bone lesions, which may increase sensitivity for bone metastases, but on the other hand may also increase specificity by identifying false positive lesions.

Fig. 11.10 Moderate focal uptake of [68Ga]-DOTATOC in the thoracic spine (MIP, lateral view). No other pathologic lesions were observed in the PET data

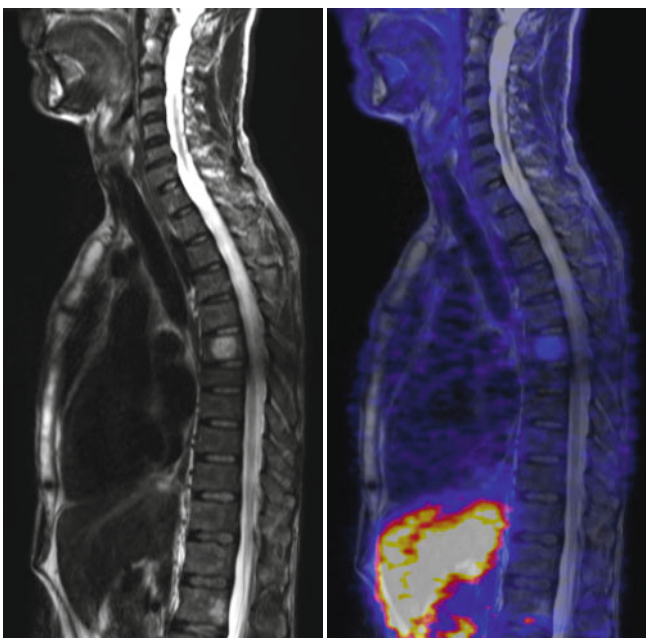

Fig. 11.11 The focal lesion projects on a hyperintense lesion in the 8th thoracal vertebra on the T2w images. *Left*: MRI T2w, sagittal view. *Right*: PET/MR fusion, sagittal view

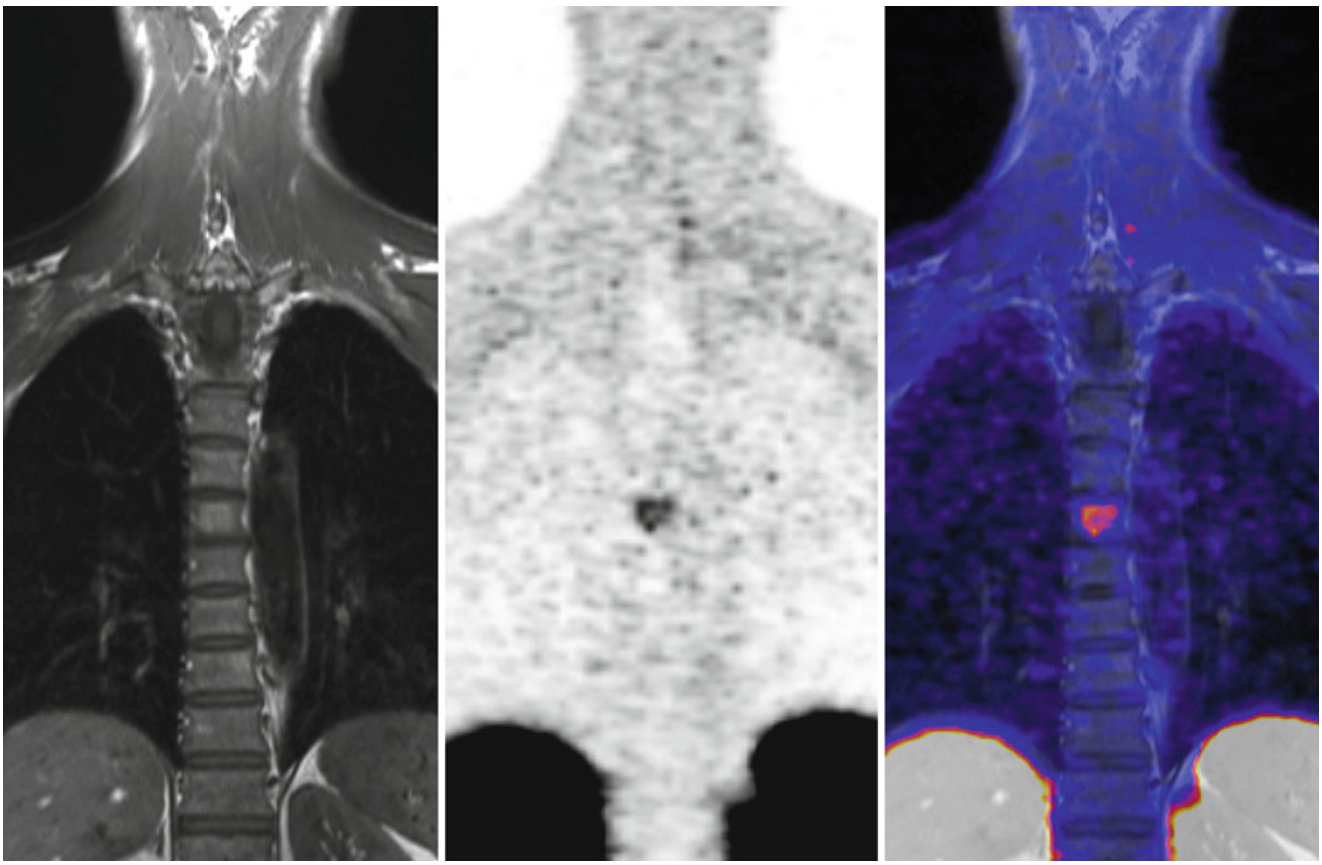

Fig. 11.12 The same lesion (8th thoracal vertebra) on T1w MRI images. *Left*: coronal T1w MRI. *Middle*: PET, coronal view. *Right*: PET/MR fusion

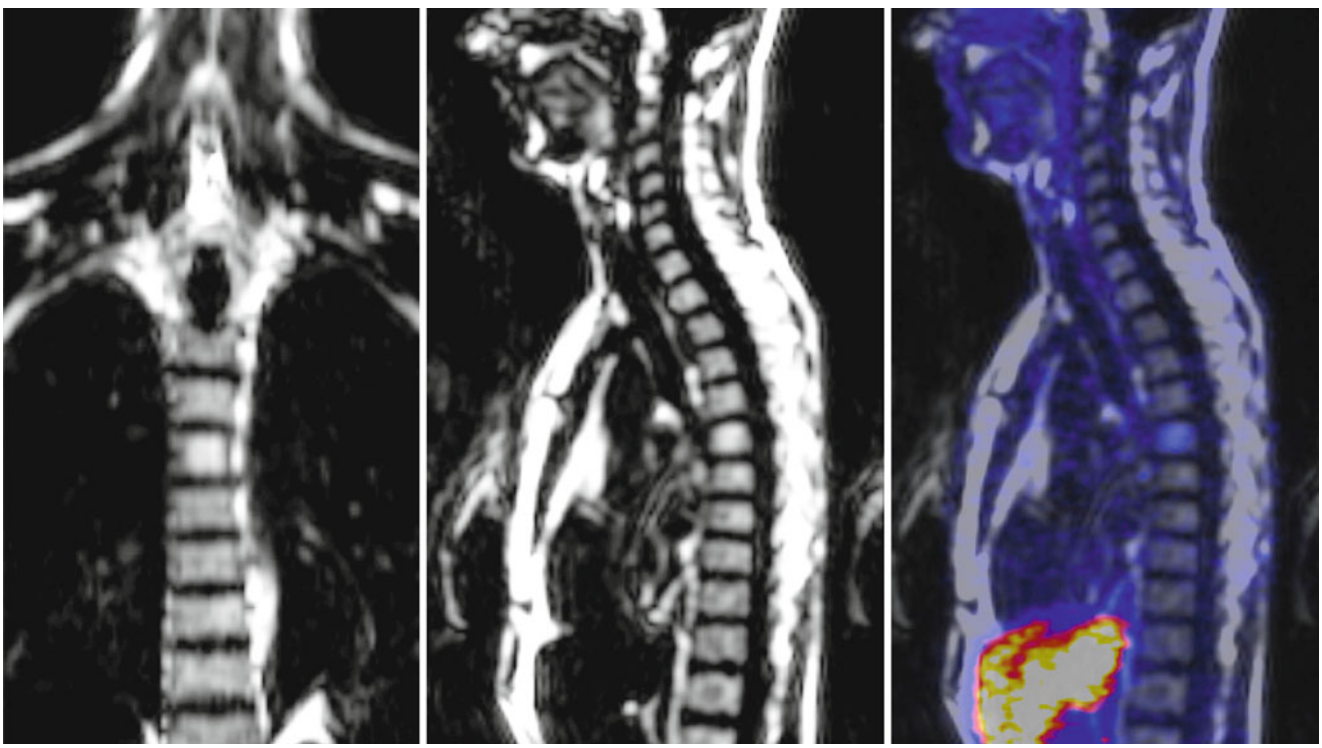

Fig. 11.13 The lesion in the 8th thoracal vertebra is also hyperintense on the fat-weighted Dixon images (acquired for attenuation correction), consistent with high fat content, consistent with a hemangioma. *Left*: coronal fat-weighted Dixon image. *Middle*: sagittal fat-weighted Dixon image. *Right*: sagittal PET/MR fusion

Papillary Thyroid Cancer

Clinical History

Twenty-three-year-old male patient with papillary thyroid cancer pT3pN1R0 (03/2012). He received ^{131}I therapy for ablation in April 2012. He presented with increased Tg levels (hTg: 3.6 ng/ml, TSH > 100 μIU/ml) and therefore ^{131}I scintigraphy after administration of 40 MBq ^{131}I was performed (Fig. 11.14). To exclude FDG-avid, ^{131}I negative metastases, 18F-FDG PET/MR was performed while planning a second ^{131}I therapy.

Imaging Technique

PET/MR 97 min p.i. of 317 MBq 18F-FDG, 70 kg, 5 bed positions 4 min per bed position. T1 VIBE Dixon for attenuation correction.

MR component: neck: ax T2 STIR, ax T1 TSE –/+ Gd cor T1 SPIR post Gd trunk: ax T1 VIBE fs.

Findings

Diagnostic ^{131}I scan (Fig. 11.14) and 18F-FDG PET/MR (Fig. 11.15) do not exhibit any pathological increased focal uptake. However in the ^{131}I planar and SPECT/CT scan performed after treatment with 206 mCi of ^{131}I increased focal ^{131}I uptake is shown in right cervical lymph nodes (Fig. 11.16). The lymph nodes cannot be distinguished on CT images of SPECT/CT, however they can be identified on MR images of PET/MR (Fig. 11.17).

Teaching Points

When exact anatomical localization of thyroid cancer manifestations is an issue, the MR component of PET/MR can be a valuable tool as the diagnostic performance of CT is limited in this condition due to the inability to use contrast enhancement. Latter would lead to iodine contamination limiting treatment with ^{131}I. Further, iodine negative 18F-FDG avid lesions could be identified with PET/MR.

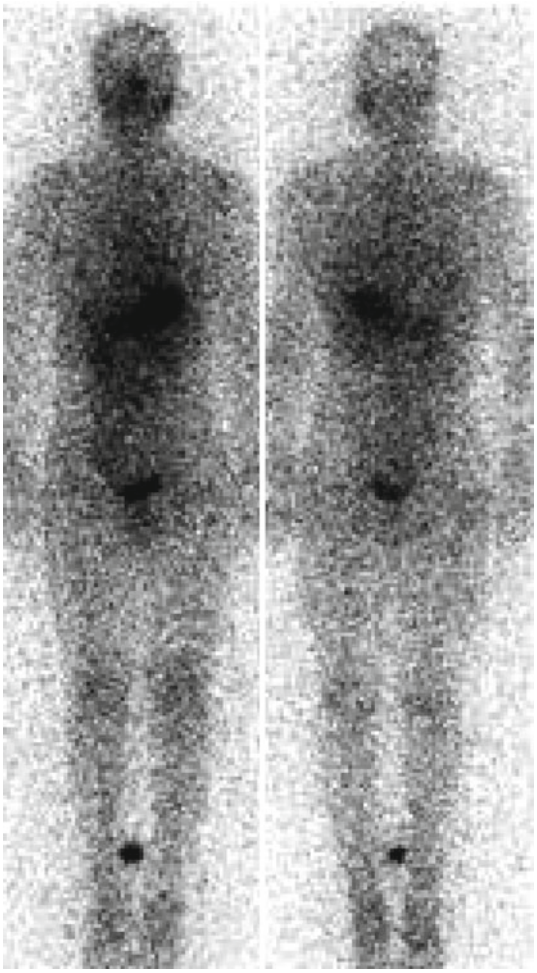

Fig. 11.14 Diagnostic ^{131}I scan (40 MBq ^{131}I) does not show any pathological focal ^{131}I uptake

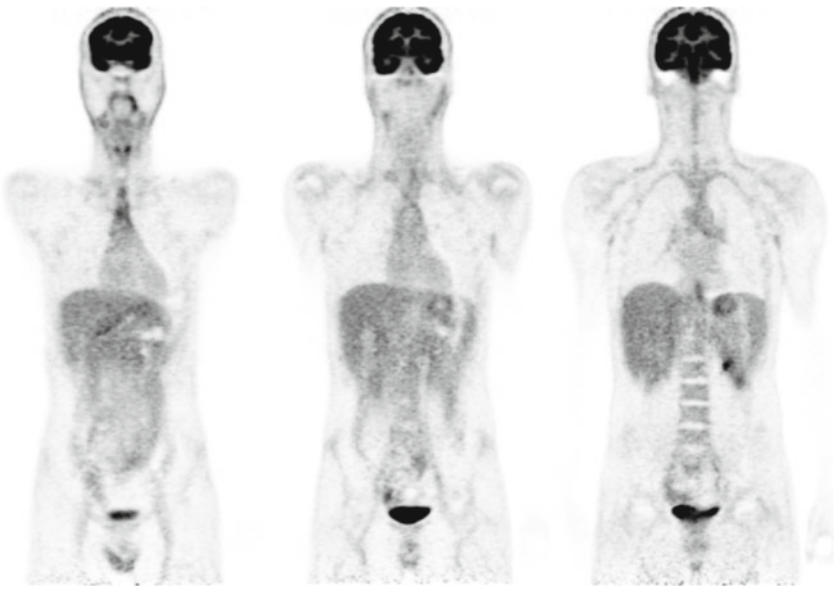

Fig. 11.15 Three coronal planes of the PET component of PET/MR without any evidence for a correlate for the increased hTg level

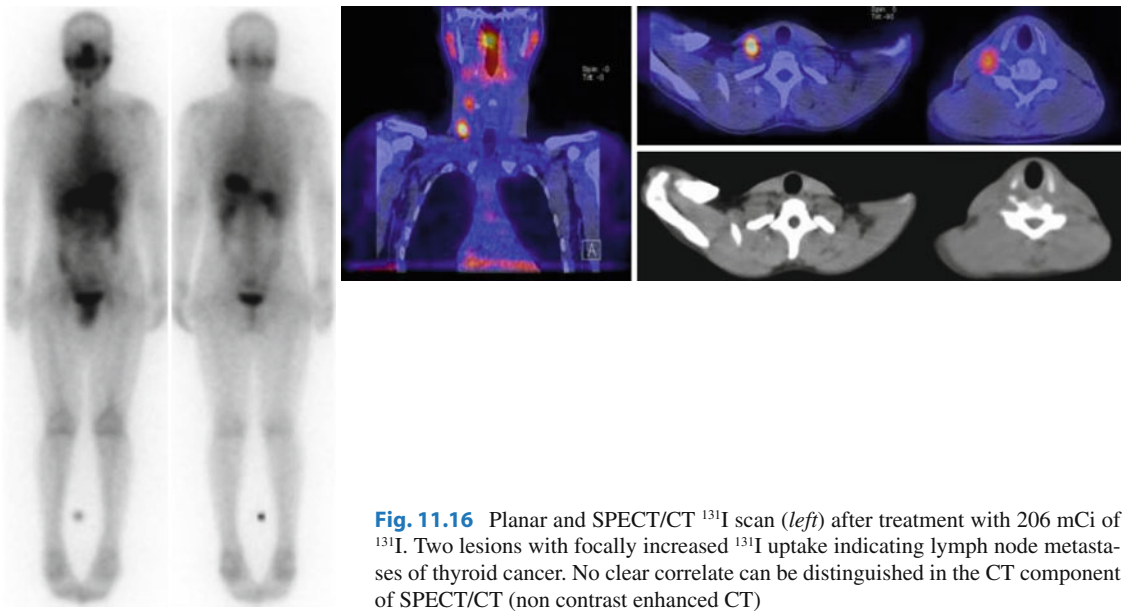

Fig. 11.16 Planar and SPECT/CT ^{131}I scan (*left*) after treatment with 206 mCi of ^{131}I. Two lesions with focally increased ^{131}I uptake indicating lymph node metastases of thyroid cancer. No clear correlate can be distinguished in the CT component of SPECT/CT (non contrast enhanced CT)

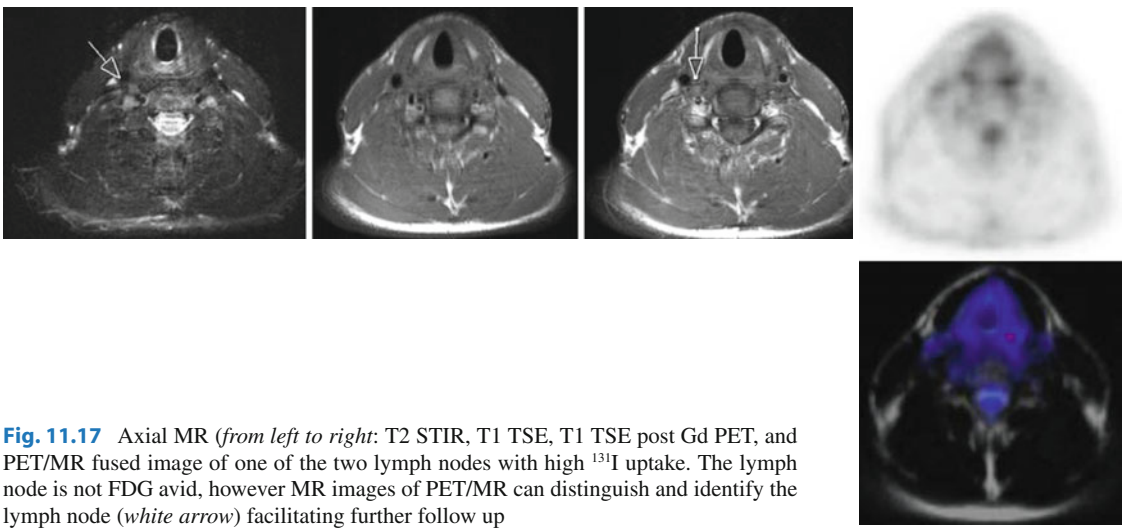

Fig. 11.17 Axial MR (*from left to right*: T2 STIR, T1 TSE, T1 TSE post Gd PET, and PET/MR fused image of one of the two lymph nodes with high ^{131}I uptake. The lymph node is not FDG avid, however MR images of PET/MR can distinguish and identify the lymph node (*white arrow*) facilitating further follow up

Lymph Node Metastasis of Thyroid Cancer

Clinical History

Seventy-six-year-old male patient after thyreoidectomy and ablative radioiodine treatment because of papillary thyroid cancer pT3pN1b(2/37)R0. Patient is referred for restaging due to a sonographically conspicuous lymph node in the left supraclavicular region. Thyreoglobulin in serum is not elevated, however there are thyreoglobulin antibodies. Diagnostic 131I scintigraphy (planar and SPECT/CT) with 379 MBq 131I and 18F-FDG PET/MR were performed.

Imaging Technique

PET/MR 78 min p.i. of 428 MBq 18F-FDG, 91 kg, 4 bed positions 4 min per bed position. T1 VIBE Dixon for attenuation correction.

MR component: Neck: ax T2 STIR, ax T1 TSE –/+ GD, cor T1 SPIR post GD, cor T1 TSE, trunk: ax T1 VIBE fs.

Findings

131I scintigraphy did not show any pathological focal uptake, however CT component of SPECT/CT demonstrates an enlarged lymph node in the left supraclavicular region (Fig. 11.18). PET/MR confirms the enlarged lymph node exhibiting an increased glucose utilization, suspicious for malignancy. No other lesions suspicious for malignant manifestations were shown (Figs. 11.19 and 11.20). Whole body PET/MR showed suspicion of a singular metastasis of thyroid cancer. Surgical lymph node excision followed, histopathology confirmed metastasis of papillary thyroid cancer.

Teaching Points

PET/MR is a valuable tool for evaluating iodine negative thyroid cancer. The whole body imaging capability of this technique allows better screening of distant lesions and adjustment of targeted therapy.

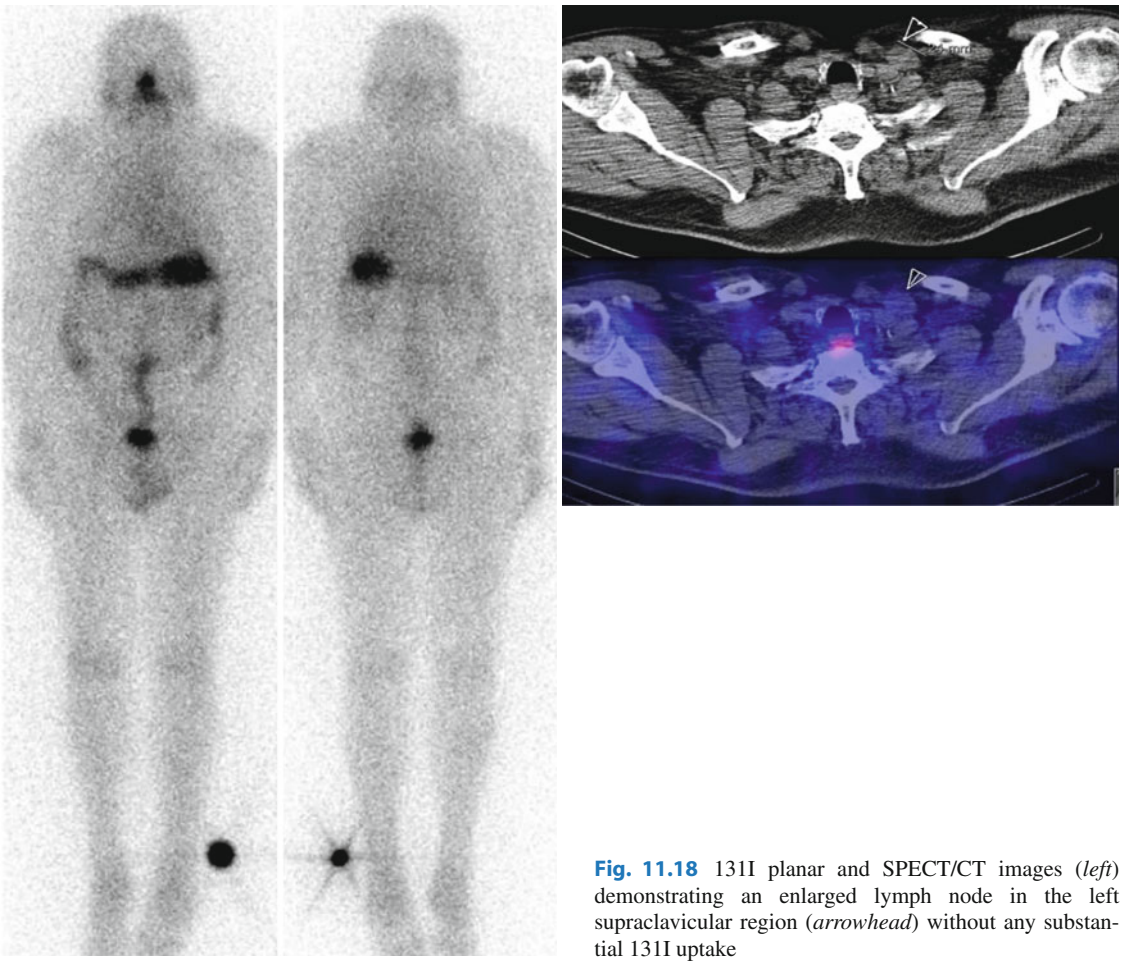

Fig. 11.18 131I planar and SPECT/CT images (*left*) demonstrating an enlarged lymph node in the left supraclavicular region (*arrowhead*) without any substantial 131I uptake

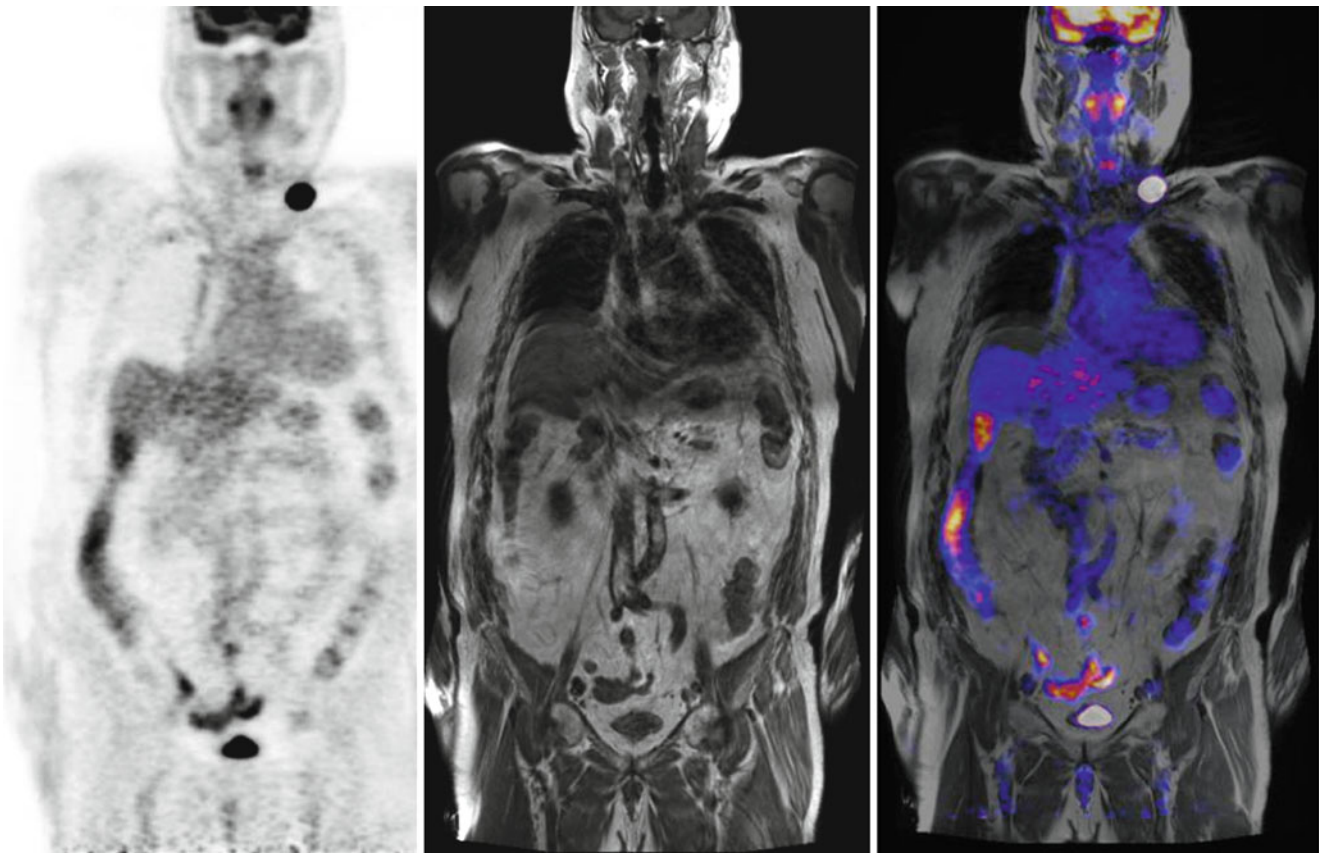

Fig. 11.19 PET, cor T1 TSE and fused image of the 18F-FDG PET/MR study. Increased focal uptake in the left supraclavicular lymph node, indicative of metastatic disease. No other suspicious lesions were observed

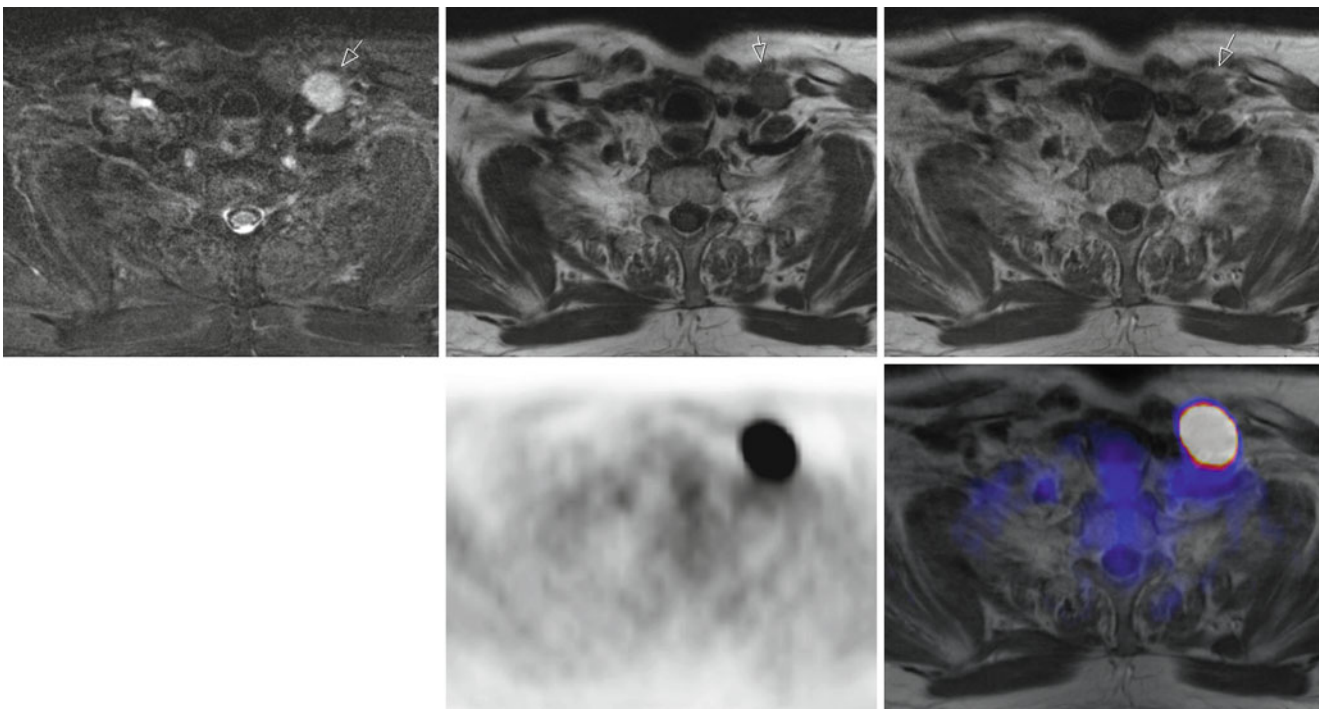

Fig. 11.20 ax T2 STIR, ax T1 TSE, ax T1 TSE post Gd, ax PET and ax fused PET/MR of the PET/MR study. The pathologically enlarged lymph node shows the typical T2 hyperintense/T1 isointense signal (*arrows*)

Hürthle Cell Thyroid Cancer

Clinical History

Restaging of a 67 year old male patient with Hürthle cell thyroid carcinoma after thyroidectomy, pT4pN0(0/16)R1, and radioiodine treatment for ablation, presenting with increasing thyreoglobulin levels (4 ng/ml) and negative post-therapeutic 131I scintigraphy.

Imaging Technique

PET/MR 90 min p.i. of 448 MBq 18F-FDG, 92 kg, 4 bed positions 4 min per bed position. T1 VIBE Dixon for attenuation correction.

MR component: neck: ax T2 STIR, ax T1 TSE –/+ Gd cor T1 STIR post Gd cor T1 TSE.

Findings

Increased focal 18F-FDG uptake in the region of the formal right thyroid bed indicating local recurrence of the thyroid carcinoma (Figs. 11.21 and 11.22). No other suspicious lesions were observed.

Teaching Points

This case emphasizes the value of PET/MR in iodine negative manifestations of thyroid cancer such as in Hürthle cell carcinoma. The excellent tumor/background ratio of the lesion demonstrated in the PET component of PET/MR facilitates detection of the lesion.

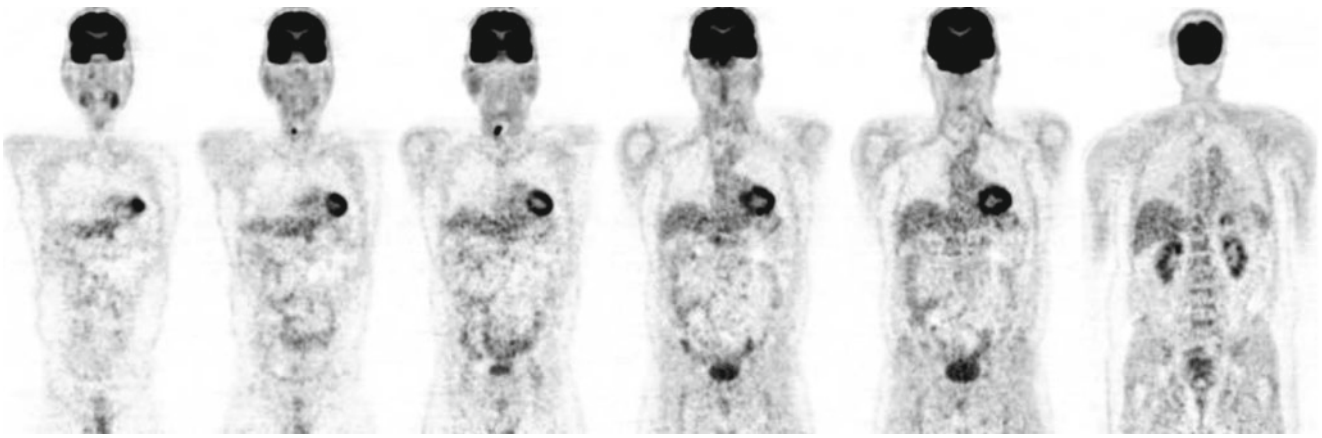

Fig. 11.21 Different coronal levels (from ventral to dorsal) of the PET component of the PET/MR. Increased focal uptake on the right formal thyroid bed indicating local recurrence.

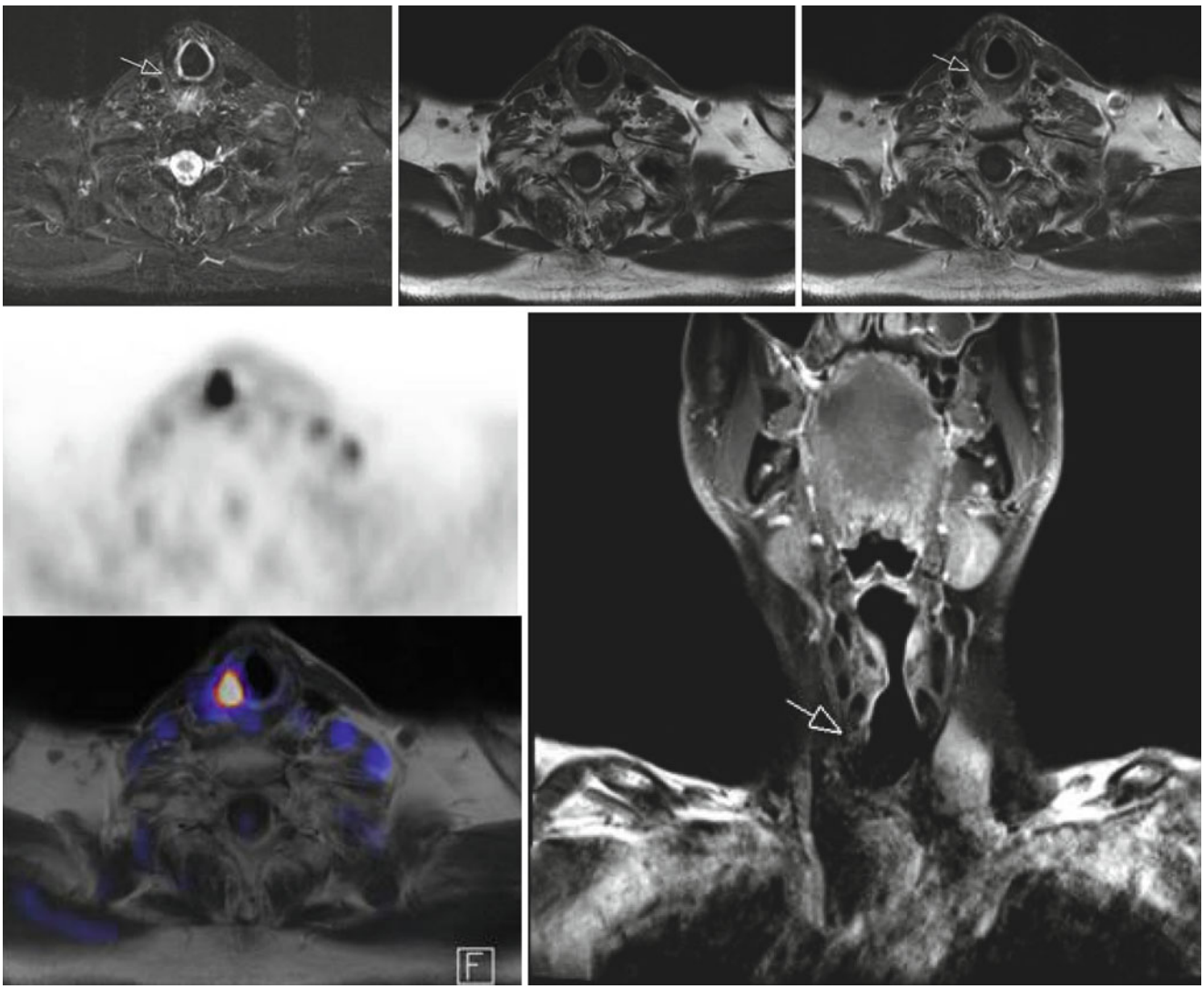

Fig. 11.22 *Upper row*: image of ax T2 STIR, ax T1 TSE and ax T1 TSE post Gd showing a T2 hyperintense signal alteration in the formal right thyroid bed enhancing after contrast media application (*arrows*). *Lower row*: image of ax PET and ax PET/MR fusion as well as cor T1 SPIR post Gd showing a contrast enhancing signal alteration in the formal thyroid bed (*arrow*) corresponding to the hypermetabolic lesion demonstrated in PET. Please note the very high tumor/background ratio in the PET image facilitating detection of local recurrence

References

1. Macapinlac HA (2001) Clinical usefulness of FDG PET in differentiated thyroid cancer. J Nucl Med 42(1):77–78
2. Schlüter B, Bohuslavizki KH, Beyer W, Plotkin M, Buchert R, Clausen M (2001) Impact of FDG PET on patients with differentiated thyroid cancer who present with elevated thyroglobulin and negative 131I scan. J Nucl Med 42(1):71–76
3. Wang W, Macapinlac H, Larson SM, Yeh SDJ, Akhurst T, Finn RD et al (1999) [18F]-2-Fluoro-2-deoxy-d-glucose positron emission tomography localizes residual thyroid cancer in patients with negative diagnostic 131I whole body scans and elevated serum thyroglobulin levels. JCEM 84(7):2291–2302
4. Grünwald F, Kälicke T, Feine U, Lietzenmayer R, Scheidhauer K, Dietlein M et al (1999) Fluorine-18 fluorodeoxyglucose positron emission tomography in thyroid cancer: results of a multicentre study. Eur J Nucl Med 26(12):1547–1552
5. Seiboth L, Van Nostrand D, Wartofsky L, Ousman Y, Jonklaas J, Butler C et al (2008) Utility of PET/neck MRI digital fusion images in the management of recurrent or persistent thyroid cancer. Thyroid 18(2):103–111
6. Mosci C, Iagaru A (2011) PET/CT imaging of thyroid cancer. Clin Nucl Med 36(12):e180–e185
7. Abraham T, Schöder H (2011) Thyroid cancer—indications and opportunities for positron emission tomography/computed tomography imaging. Semin Nucl Med 41(2):121–138
8. Buchmann I, Henze M, Engelbrecht S, Eisenhut M, Runz A, Schäfer M et al (2007) Comparison of 68Ga-DOTATOC PET and 111In-DTPAOC (Octreoscan) SPECT in patients with neuroendocrine tumours. Eur J Nucl Med Mo Imaging 34(10): 1617–1626
9. Schreiter NF, Nogami M, Steffen I, Pape U-F, Hamm B, Brenner W et al (2012) Evaluation of the potential of PET/MRI fusion for detection of liver metastases in patients with neuroendocrine tumours. Eur Radiol 22(2):458–467
10. Ruf J, Lopez Hänninen E, Böhmig M, Koch I, Denecke T, Plotkin M et al (2006) Impact of FDG-PET/MRI image fusion on the detection of pancreatic cancer. Pancreatology 6(6):512–519
11. Tatsumi M, Isohashi K, Onishi H, Hori M, Kim T, Higuchi I et al (2011) 18F-FDG PET/MRI fusion in characterizing pancreatic tumors: comparison to PET/CT. Int J Clin Oncol 16(4):408–415
12. Kalra MK, Maher MM, Mueller PR, Saini S (2003) State-of-the-art imaging of pancreatic neoplasms. Br J Radiol 76(912): 857–865
13. Fidler JL, Johnson CD (2001) Imaging of neuroendocrine tumors of the pancreas. Int J Gastrointest Cancer 30(1–2):73–85